PCCP

PAPER

View Article Online
View Journal | View Issue

Cite this: *Phys. Chem. Chem. Phys.*, 2014, **16**, 5824

Hydration properties of Cm(III) and Th(IV) combining coordination free energy profiles with electronic structure analysis†

Riccardo Spezia,*[ab] Yannick Jeanvoine,[ab] Cesar Beuchat,[c] Laura Gagliardi[d] and Rodolphe Vuilleumier[efg]

Received 24th November 2013,
Accepted 29th January 2014

DOI: 10.1039/c3cp54958e

www.rsc.org/pccp

The hydration structure of two actinoid ions of different charge, Cm(III) and Th(IV), was investigated. Density Functional Theory, DFT-based molecular dynamics and the single sweep method were used to obtain free energy landscapes of ion–water coordination. Free energy curves as a function of the ion–water coordination number were obtained for both ions. The number of water molecules in the first coordination shell of Cm(III) varies between 8 and 10. For Th(IV), on the other hand, the 9-fold structure is stable and only the 10-fold structure seems to be accessible with a small but non-negligible free energy barrier. Finally, by combining molecular dynamics simulations with electronic structure calculations, we showed that the differences between Cm(III) and Th(IV) are mainly due to electrostatic effects. Cm(III) is less charged and it has fewer water molecules in its first shell, while Th(IV) has more water molecules because of a stronger electrostatic interaction.

1. Introduction

The hydration of highly charged ions is an interesting problem that has been studied both experimentally and theoretically.[1–4] Molecular dynamics simulations have been employed to explore the ion–water distance, coordination number, ionic diffusion, and first shell water exchange dynamics.[5–11] Exchange dynamics is crucial to characterize the hydration structure and transport properties[12] of highly charged ions and it is thus important to take into account the coexistence of different coordination numbers.[13,14]

Density Functional Theory (DFT)-based molecular dynamics simulations of ion hydration in liquid water can at the same time describe the interactions from first principles and explicitly consider bulk properties. The main problem with such methods is that the affordable simulation time length (of the order of tens of picoseconds) is often shorter than the time required for exchange dynamics of first shell water molecules to occur.[2] As a consequence, only very fast processes can be observed. For this reason, DFT-based dynamics often provide less information than classical dynamics based on a well parameterized force field.[15,16] On the other hand, using DFT is often tempting since the results are independent of a specific parameterization.

A way of combining the information coming from a DFT description and the information on coordination structure under bulk conditions is to obtain the free energy profile corresponding to different coordination numbers (*i.e.* free energy as a function of water molecules in the first hydration shell). Amongst different possible algorithms to perform such free energy calculations, the single sweep method (SSM)[17] is very appealing, since it is well coupled with DFT-based (or more in general computationally expensive) molecular dynamics to overcome free energy barriers implying time scales unaffordable by unbiased DFT-dynamics.[18–22] SSM is one of the possible enhanced sampling methods to get information on free energy profiles. Metadynamics, based on the filling of the free energy surface by the system,[23] is a different (but similar somehow in spirit) method that was also applied to provide insights on ion hydration.[24,25]

In this study we have coupled SSM with DFT molecular dynamics simulations to compare the hydration properties of two actinoid ions in liquid water, Cm(III) and Th(IV). We recently addressed their hydration properties from polarizable molecular dynamics and successfully explained EXAFS data.[26,27] In the

[a] *CNRS, UMR 8587, France*
[b] *Université d'Evry Val d'Essonne, Laboratoire Analyse et Modélisation pour la Biologie et l'Environnement, Bd. F.Mitterrand, 91025 Evry Cedex, France. E-mail: riccardo.spezia@univ-evry.fr*
[c] *Department of Physical Chemistry, University of Geneva, 30 Quai Ernest Ansermet, CH-1211 Geneva, Switzerland*
[d] *Department of Chemistry, Chemical Theory Center, and Supercomputing Institute, University of Minnesota, 207 Pleasant Street SE, Minneapolis, Minnesota 55455-0431, USA*
[e] *Ecole Normale Supérieure, Département de Chimie, 24, rue Lhomond, 75005 Paris, France*
[f] *UPMC, Univ Paris 06, 4, Place Jussieu, 75005 Paris, France*
[g] *CNRS-ENS-UPMC, UMR 8640, France*

† Electronic supplementary information (ESI) available. See DOI: 10.1039/c3cp54958e

present paper we show how DFT dynamics (free of any parameterization) provides information on the ion coordination and on ion–water interaction. In particular we focus on the different solvation behaviors of two actinoid ions by using DFT. Note that Cm(III) and Th(IV) were also studied by employing accurate potentials derived from high level *ab initio* calculations.[28,29] For Cm(III), simulations from various groups confirmed the experimental results that the coordination in water is an equilibrium between 9-fold and 8-fold structures[4,26–28,30–32] with a preference for the 9-fold one.[33] DFT-based dynamics with the PBE functional by Atta-Fynn *et al.*[34] found a coordination number of 8. More recently, these authors, by employing metadynamics, showed that the 9-fold structure is stabilized by counterions like perchlorates (ClO_4^-).[35] For Th(IV), on the other hand, there is still some controversy: some simulations and experiments found that 9- and 10-fold structures are accessible,[36–39] with a preference for the 9-fold one,[40] while other simulations suggest 8-fold and 9-fold structures.[29,41] The free energy surfaces as a function of ion–water coordination number obtained at the DFT level can shed light on the question. Note that DFT simulations performed without any technique that accelerates the barrier crossings can provide coordination numbers that are meta-stable states, as we obtained in the case of La(III) and Th(IV) in water.[15,39] Thus, in DFT-based molecular dynamics simulations where the water coordination number is let free to evolve without any bias, it is always questionable that when a given coordination number is obtained this corresponds to a stable or to a meta-stable state, even from relatively long simulations (tens of ps) that are too short to be statistically representative of first hydration shell self-exchange dynamics. By calculating free energy surfaces using DFT-based simulations we can provide a full picture of hydration of such ions.

From a fundamental point of view, the interaction between actinoid ions and water is of interest since 5f electrons are more diffuse than the corresponding 4f electrons of the lanthanoid series and thus they can in principle interact differently with water. Here, we coupled the study of the water coordination free energy surface with electronic structure analysis conducted by employing both DFT and wave-function methods, MP2 and CASSCF/CASPT2. In particular, we describe the nature of the ion–water interactions obtained both from DFT and MP2 and CASSCF/CASPT2 theories by using the representative structure on the coordination free energy profile obtained by SSM-DFT simulations.

The overall purpose of this study is to compare two prototypical 5f ions, Cm(III) and Th(IV), with different charge, and the way they interact with water molecules from both thermodynamics and electronic structure approaches. In addition to our previous studies,[26,28,39] here we provide a quantitative description of free energy differences and barriers between different coordination numbers and make the connection with electronic properties that are studied as a function of hydration structure, by selecting the key structures (minima and saddle points) along the coordination free energy landscapes. Furthermore, we show for the first time that the single sweep method can be used to study the subtle problem of ion hydration.

The remainder of the paper is organized as follows. In Section 2 we describe the methodological details. In Section 3 we present and discuss the results. Finally, in Section 4 we offer some conclusions.

2. Methods

2.1. DFT-based molecular dynamics and free energy calculations

The free energy surfaces as a function of the number of water molecules around Cm(III) and Th(IV) were obtained for both systems *via* the single-sweep method (SSM)[17,42] coupled with Car–Parrinello Molecular Dynamics[43] (CPMD). We use DFT-based molecular dynamics with plane wave basis sets and pseudo-potentials (PPs) to represent core electrons. The BLYP functional[44,45] was used with a 110 Ry cut-off in the plane waves (PWs) representation. For Th(IV) we used the Martins–Troullier[46] pseudo-potential we have recently reported[39] and for Cm(III) we have developed a similar semicore Martins–Troullier pseudo-potential as follows. The reference configuration used to generate the PP for Cm was Cm(III), *i.e.* $5f^7 6s^2 6p^6 6d^0$ for outer orbitals. The orbitals 6s, 6p, 6d and 5f were included in the PP with cut-offs of 1.33, 1.59, 2.36 and 1.20 a.u., respectively. When using this PP with PWs, the semilocal Kleinman–Bylander[47] form was used with the *p* channel as the local channel (both for Cm and Th). Cm(III) is a $5f^7$ system and we considered the high spin state (eight-fold multiplicity) within the local spin density. Th(IV) on the other hand is a closed shell ion. For water we used standard Martins–Trouiller pseudo-potentials with Kleinman–Bylander projection as routinely done.[48] Note that in some cases using dispersion corrected atom-centered pseudo-potentials (DCACP)[49] it is possible to improve the description of water (that at the BLYP level is overstructured and diffuses slowly), as done, for example, in the case of the Br^- ion in water[50] that compares better with EXAFS experiments than without dispersion.[51] Here, anyway, we used the standard pseudo-potential since we want to be coherent with our previous study on Th(IV) in water that provided structural properties in agreement with EXAFS experiments.[39]

Each Cm(III) and Th(IV) ion was immersed in a water box of 12.4325 Å edge containing 64 water molecules that was previously used to study Th(IV) in water.[39] This corresponds to the size employed in a pure water calculation with 64 water molecules at ambient pressure and with a density of 1 g cm^{-3}. We thus used the same box previously employed for Th(IV) in both cases. The equations of motion were solved numerically with a time step of 2 a.u. (=0.048378 fs) and a fictitious mass of 200 a.u.

To obtain the free energy curves using the single sweep method, we proceeded as follows. We first (step 1) defined a reaction coordinate (RC), in our case the water coordination number (CN) around the ion, by means of a Fermi function:

$$\mathrm{CN} = \sum_{j_{\mathrm{sp}}=1}^{N_{\mathrm{sp}}} \frac{1}{1 + e^{k\left(d_{Mj_{\mathrm{sp}}} - d^0\right)}} \qquad (1)$$

where j_{sp} runs over the oxygen atoms (N_{sp}), $d_{Mj_{sp}}$ is the distance between the central ion and oxygen atoms, k = 2.0 a.u. and d^0 = 3.5 Å. Note that these parameters are very similar to what was recently used by Atta-Fynn *et al.* for studying the hydration structure of Cm(III) using metadynamics.[35]

We then (step 2) performed a molecular dynamics (MD) run where we set the temperature on the RC to 5000 K by means of a Langevin thermostat. This temperature accelerated evolution of an extended system, including the collective variable as a dynamical variable (and thus only the dynamical variable corresponding to the defined RC evolves at high temperature), is able to overcome barriers and efficiently explore the free energy landscape.[52] The Nosé–Hoover[53] thermostat is applied to other coordinates with the target temperature of 300 K. In order to improve the reactive space sampling, we run different single-sweep simulations using different initial structures: 10-, 9- and 8-fold coordination for Th(IV) and 9- and 8-fold coordination for Cm(III). In this way, we let the system span as much as possible the RC. Finally (step 3), we selected points on the RC as obtained from the previous temperature accelerated molecular dynamics. At these centers, the mean force on the constraint is computed by performing MD simulations where a constrain is imposed at each value of the RC for an overall of about 35 ps for Th(IV) and 25 ps for Cm(III) and computed the mean force on the constrain. This corresponds to use as constrain the same Fermi function (eqn (1)) used to define the reaction coordinate. Then, given the centers and the mean force at the values of the collective variable, the free energy is reconstructed using an interpolation scheme where the free energy is expressed as a sum of Gaussian centered at the grid points. More details on the procedure can be found elsewhere.[42,54]

All simulations were performed by means of CPMD code.[55]

2.2. Electronic structure calculations

Electronic structure calculations were performed on selected cluster structures obtained from molecular dynamics simulations using both density functional theory, DFT, and wave-function based methods, single-reference perturbation theory, MP2 and multireference perturbation theory, CASPT2.

In the DFT calculations we employed the ECP60MWB_SEG Stuttgart basis set[56,57] with the energy-consistent pseudopotentials (ECP) for Cm and Th, while for O and H we used the 6-31+G(d,p) basis set. The ECP60MWB_SEG uses 60 core electrons, multielectron fit (M) and quasirelativistic reference data (WB). Calculations were performed using three different functionals: BLYP,[44,45] a 'pure' GGA functional, B3LYP,[58] a hybrid GGA functional and M05-2X,[59] a meta-hybrid functional where the Hartree–Fock exchange is double with respect to the original M05. BLYP was chosen since it is the same functional used in molecular dynamics, B3LYP since it is probably one of the most popular functionals and M05-2X since it has been shown to perform well in cases where B3LYP seems to fail.[60,61]

Natural Bond Orbital (NBO) analysis[62–64] of the bonds between the water molecules and the actinoid cations was also performed using the DFT densities as obtained using different functionals. These calculations were performed by using the NBO5.9 code.[65]

The MP2 and CASPT2 calculations were performed using the software MOLCAS-7.6.[66] The CASSCF method[67] was used to generate molecular orbitals and reference functions for subsequent multiconfigurational, second-order perturbation calculations of the dynamic correlation energy (CASPT2).[68] Scalar relativistic effects were included using the Douglas–Kroll–Hess Hamiltonian and relativistic ANO-RCC basis sets[69] of triple-ζ quality. In the CASSCF calculations, the active space was formed by the Ac 5f orbitals. In the Th^{4+} case, corresponding to the valence electronic configuration $5f^0$, the active space was thus empty, and the calculation was reduced to a conventional Hartree–Fock followed by perturbation theory to second order, MP2, calculation. In the Cm^{3+} case, we considered an active space of 7 electrons in 12 orbitals, corresponding to the valence electronic configuration $5f^7 6d^0$. The combination of the CASSCF/CASPT2 approach with ANO-RCC basis sets has been successful in studying many actinide and lanthanide containing systems.[70–78]

3. Results and discussion

3.1. Free energy profile

From SSM simulations we obtained the free energy profile as a function of the first shell coordination number (CN). These curves are reported in Fig. 1.

We should discuss three types of coordination-number quantifiers that are used in the following. (i) The first, here called CN, is defined by eqn (1), *i.e.* it is obtained by the Fermi function that is a continuous function. Thus, it can take on non-integer values, since the Fermi function is explicitly designed to avoid discontinuities. (ii) The number of water molecules obtained just by counting how many water molecules are present in the first shell from constrained structures corresponding to each value of CN. This number, NW, is by definition an integer and it corresponds to visual inspection of the first shell.

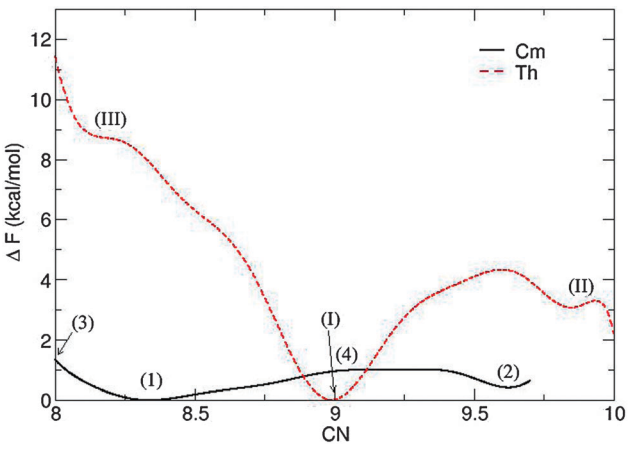

Fig. 1 Free energy profile as a function of the reaction coordinate defined by eqn (1). The black solid line shows the results for Cm(III) and the red dashed line shows the results for Th(IV). Selected points for Cm(III) are in arabic numbers, while those for Th(IV) are in roman numerals.

In some cases we can adopt an $n + m$ nomenclature, where n is the number of water molecules in the first shell and m is the number in between the first and second shells (shells are formally defined from the $g(r)$ minima). (iii) The average coordination number can be obtained by integrating the ion–water radial distribution function, $g(r)$. This quantity can also assume non-integer values, but not necessarily the same as that of CN defined by eqn (1).

We first comment on the Cm(III) free energy surface. The curve shows two minima, the first at CN = 8.3, corresponding to a structure with NW = 8 + 1, and the second at CN = 9.6, corresponding to NW = 10. The energy difference between the two minima is less than 1 kcal mol^{-1} and the barrier between them is also very small ($\sim$1 kcal mol^{-1}), corresponding to CN = 9 and NW = 9 + 1. The structure corresponding to CN = 8 and NW = 8 is also very close in energy. This means that the system is almost free to move between 8- and 10-fold coordination at room temperature. Snapshots from each constrained simulation are shown in Fig. 2: structure (1) corresponds to CN = 8.3 (NW = 8 + 1), structure (2) to CN = 9.6 (NW = 10), structure (3) to CN = 8.0 (NW = 8) and structure (4) to CN = 9.0 (NW = 9 + 1).

A comparison of our free energy curves with those obtained by Atta-Fynn *et al.*[35] shows similar energy differences between 8- and 9-fold structures (1 kcal mol^{-1} *vs.* 3 kcal mol^{-1}) and similar barriers between those two states (1 kcal mol^{-1} *vs.* about 4 kcal mol^{-1}). The small differences between the two studies can be attributed to the different functionals employed (BLYP *vs.* PBE) rather than to the procedure for obtaining free energy curves. Our results provide a quantitative estimation of the interconversion between the 9-fold and 8-fold structures observed by Hagberg *et al.*[28] The low barrier obtained for Cm(III) explains the relatively fast exchange obtained by classical MD simulations by Hagberg *et al.*[28] and also why the average CN changed as a function of temperature.[28]

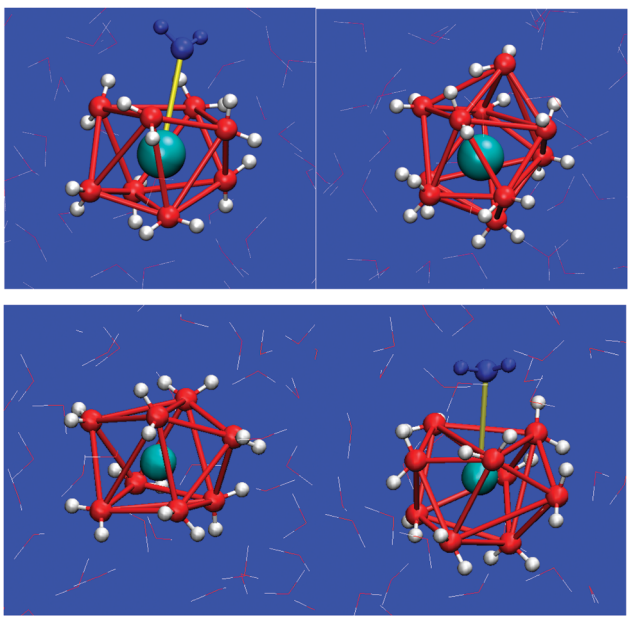

Fig. 2 Cm(III) in water snapshots from different constrained dynamics from which free energy surface is obtained. From top to bottom and left to right, we show structures corresponding to the following states on the Cm(III) free energy surface (Fig. 1): (1), (2), (3) and (4).

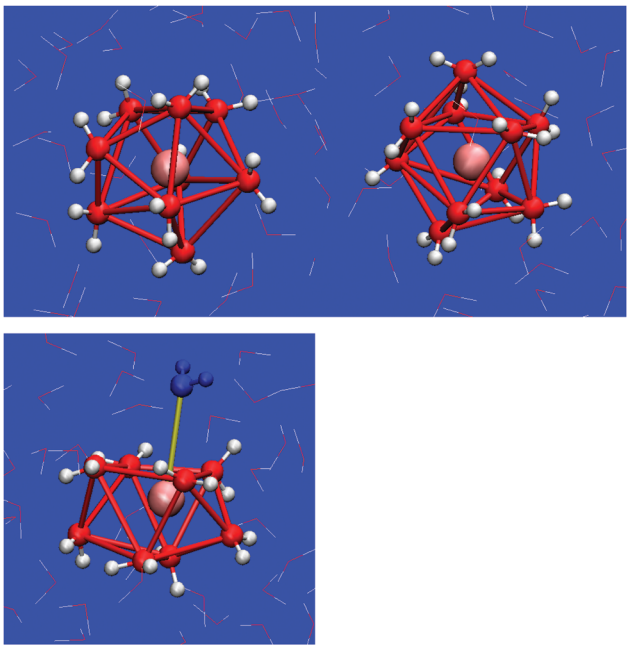

Fig. 3 Th(IV) in water snapshots from different constrained dynamics from which free energy surface is obtained. From top to bottom and left to right, we show structures corresponding to the following states on the Th(IV) free energy surface (Fig. 1): (I), (II) and (III).

The Th(IV) free energy curve is rather different compared to Cm(III). A stable state is found for CN = 9, corresponding to NW = 9, and a second minimum for CN = 9.8, corresponding to NW = 10. The free energy difference between the two states is 3 kcal mol^{-1} and the corresponding barrier is *ca.* 4 kcal mol^{-1}. The reaction path towards lower CN values presents an even higher barrier and only a flat region is observed for CN = 8.1 (corresponding to NW = 8 + 1), higher in energy of about 9 kcal mol^{-1}. Snapshots from each constrained simulation are shown in Fig. 3: structure (I) corresponds to CN = 9 (NW = 9), structure (II) to CN = 9.8 (NW = 10) and structure (III) to CN = 8.1 (NW = 8 + 1). These results are in agreement with prior unconstrained simulations coupled with EXAFS analysis,[39] which determined a CN = 9: the 9-fold structure is a thermodynamical and kinetic minimum as shown by free energy difference with respect to 10-fold structure and by the free energy barriers.

The Th(IV) coordination free energy surface shows a minimum structure that is more stable than for Cm(III), even if the differences are of the order of a few kcal mol^{-1}. Our BLYP simulations and the PBE simulations of Atta-Fynn *et al.*[35] predict a similar difference for Cm(III). Experimentally the coordination of Cm(III) should be an equilibrium between CN = 8 and CN = 9,[4,27] compatible with the low energy barrier observed in BLYP simulations. In Section 3.2 we will analyze the structures along the free energy surfaces to see if this difference in energy corresponds to a difference in structuration of the water molecules around the ion.

Furthermore, in Section 3.3 we will discuss if the observed difference can be attributed to a stronger "covalent" or electrostatic interaction between water and the ion.

3.2. Structural analysis

From the constrained molecular dynamics simulations results we selected some trajectories at different constrained values of the coordination number and analyzed them in detail. Each trajectory will be called "state" in the following since it corresponds to a unique point on the free energy surfaces in Fig. 1 and all the corresponding structures correspond to the same free energy value. We have selected the most important states for Cm(III) and Th(IV) simulations (the ones highlighted in Fig. 1) and analyzed in detail the average structural properties.

From Cm(III) simulations we have selected four states (and the corresponding simulations), with CN = 8.3, 9.6, 8.0 and 9.0, corresponding to structures (1), (2), (3) and (4) in Fig. 1 and 2. The Cm–O radial distribution functions are shown in Fig. 4. Systems (2) and (3), corresponding to NW = 10 and 8, respectively, show a stable, well defined structure around the ion, since there is a clear plateau in integrated $g(r)$ (shown in the same figure as dashed lines) at values of 10 and 8, respectively. Note that they correspond to CN values of 9.6 and 8.0, respectively. This small discrepancy between CN, NW and integrated $g(r)$ is due to their slightly different definitions, as discussed previously. On the other hand, for systems (1) and (4), their integrated $g(r)$ smoothly moves from 8 to 10. In the case of system (4), this corresponds to CN = 9 with a tenth water molecule 3.5–4 Å away from the ion, which thus also comes close to the Cm(III) ion, as shown in the snapshot of Fig. 2. This corresponds roughly to an intermediate shell, labeled 9 + 1. In the case of system (1), CN = 8.3, a ninth molecule lies 3.5–4 Å away from the ion. This also corresponds to an intermediate shell and we labeled it as 8 + 1. This 'intermediate' structure interestingly corresponds to the value of 8.3 in the minimum energy surface in Fig. 1, *i.e.* the absolute minimum in the free energy landscape obtained previously. This strengthens the picture that the Cm(III) ion does not strongly stabilize a given structure and the coordination number. This holds not only from a thermodynamic point of view (the small differences between stable states and small free energy barrier), but also from a structural point of view: the coordination number smoothly moves from 8 to 10, and the most stable state is characterized by a ninth water molecule in an intermediate shell. The most stable state is thus a state where one water molecule is not at a fixed position, but can easily move away, a picture that can be seen as the dynamical counterpart of the tetrad model proposed by Persson and co-workers in the case of lanthanoid(III) ions hydration.[79]

We can now comment on some further differences in the CN minima positions found on our free energy curve and that of Atta-Fynn *et al.*[35] In particular, they found a minimum for CN = 9 while we found CN = 9.6. As we have discussed, there is no straightforward connection between CN and the number of water molecules in the first shell (NW in the notation used by us). This comes from the use of a Fermi function (eqn (1)) in the definition of CN and this is probably on the basis of the difference between the two studies, since we used slightly different parameters in the definition of this function. As detailed in Section 3.2 and shown in Fig. 4, the CN = 9.6 simulation, that corresponds to our minimum in the free energy surface, shows a tenth water molecule that is still at a longer distance: the integrated $g(r)$ reaches a plateau at around 3.25 Å and it is in between 9 and 10 in the 2.75–3.25 Å range. This is why the Fermi function provides CN = 9.6, a value that can change if different parameters are employed. Thus, if there are differences in details, our results also show that there is an equilibrium between 8-fold and 9-fold structures. We added the possibility of forming some transient 10-fold structures, where the tenth water is in between the first and second shells.

For Th(IV) the situation is rather different. We show in Fig. 5 Th–O radial distribution function of trajectories corresponding to different states in the free energy curve. In each case, we have a well-defined depleting region between the first and second

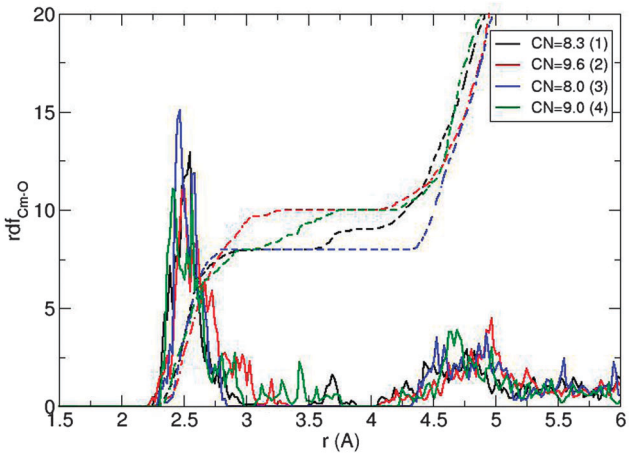

Fig. 4 Cm–O radial distribution functions (rdf) as obtained from constrained dynamics corresponding to different points on the free energy surface: (1), (2), (3) and (4).

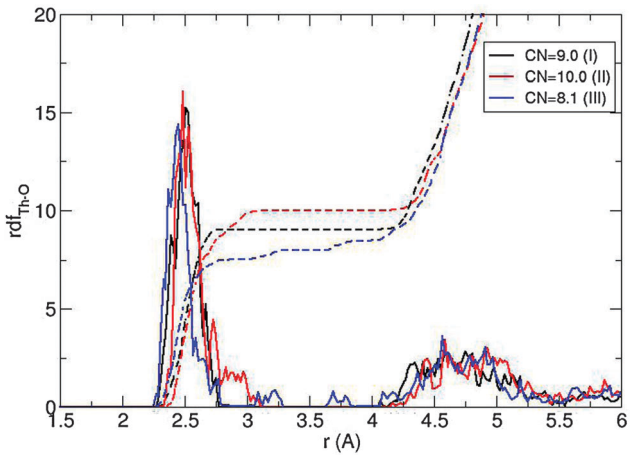

Fig. 5 Th–O radial distribution functions (rdf) as obtained from constrained dynamics corresponding to different points on the free energy surface: (I), (II) and (III).

shell where no (or few) water molecules are present, corresponding to a well defined plateau in the integrated $g(r)$. We have selected three systems: one corresponding to the minimum in the free energy surface (system (I), with CN = 9 and NW = 9), and two corresponding to NW = 8 (system (III), CN = 8.2 in the free energy surface) and NW = 10 (system (II), CN = 9.8 in the same curve). Also in this case the clear definition of well-separated thermodynamic states is reflected by well-defined structural properties. We have thus the following picture: the 9-fold structure is relatively stable and is expected to be the most relevant in solution, but also the 10-fold one is accessible. The present calculations exclude the possibility of a stable 8-fold structure: when the system is pushed towards CN = 8 (and also NW = 8) the free energy sharply increases.

The difference between the two ions is well described also from the angular distribution functions between the oxygen atoms of first shell water molecules and the central ion (O–Cm–O and O–Th–O shown in Fig. 6 and 7, respectively). In the case of Cm(III) we do not observe well defined hydration shells, corresponding to flexible coordination, while for Th(IV) the structure is much more rigid, corresponding to a strong structuration of the water molecules in the first hydration shell.

We should note that here we have considered only the hydration of bare ions in water in order to understand physical properties that are at the basis of the difference between Cm(III) and Th(IV) in pure water. Of course, these cations can hydrolyze and in the case of Th(IV) this can happen also at pH values around 1 as reported by experiments[37] and calculations.[80,81] In the present work, we focus our attention on bare ion–water complexes that can be experimentally obtained under very acidic conditions, as we have detailed in our previous study[39] where DFT-based simulations without any hydrolysis were found in good agreement with experiments under very low pH conditions. In the present simulations, we did not notice any spontaneous water hydrolysis, as obtained previously for Th(IV) and also for La(III) in water.[15] DFT-based simulations are anyhow able to provide spontaneous water hydrolysis when the reactivity is much higher, as observed for Po(IV) in water.[82] Furthermore, we have not observed any significant deformation of the water molecules around Cm(III) or Th(IV), neither a significant difference between the two systems. O–H bonds of water molecules in the first shell are very similar, slightly weakened for Th(IV) systems where the full width at half maximum is 0.073 Å while for Cm(III) systems it is 0.069 Å. This difference is too small anyway to be considered significant. Radial distribution functions between O and H atoms of water molecules in the first hydration shell of the two ions are shown in Fig. S1 of (ESI†).

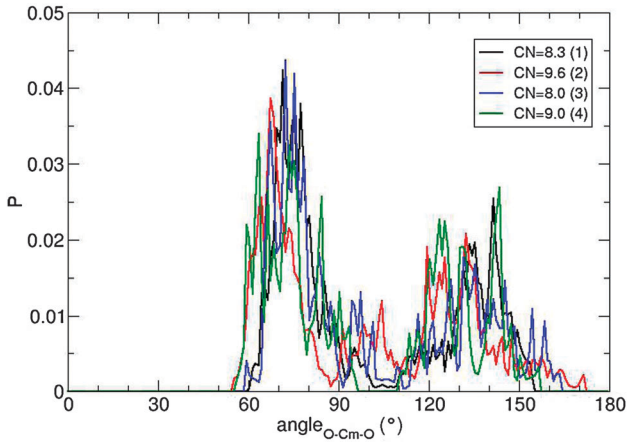

Fig. 6 O–Cm–O angular distribution function of water in the first shell, as obtained from constrained dynamics corresponding to different points on the free energy surface: (1), (2), (3) and (4).

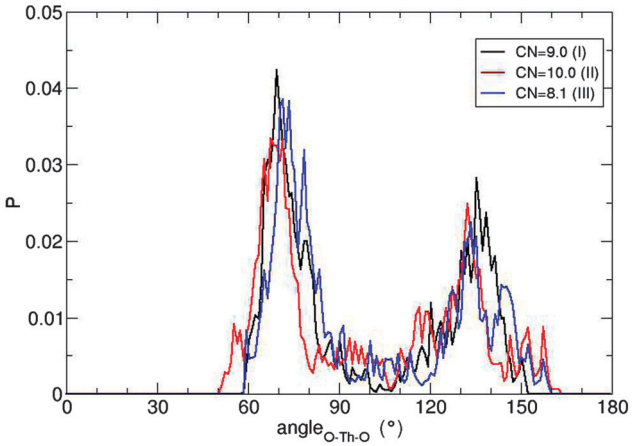

Fig. 7 O–Th–O angular distribution function of water in the first shell, as obtained from constrained dynamics corresponding to different points on the free energy surface: (I), (II) and (III).

3.3. Electronic structure

In order to validate the quality of BLYP calculations on Cm(III) and Th(IV) in water, we performed electronic structure calculations on some clusters obtained from the simulations, composed of the central ion and 8, 9 or 10 water molecules in the first shell, respectively. We employed different DFT and wave-function methods. For Cm(III) we have selected two 8-fold (Cm-8-A and Cm-8-B), one 9-fold (Cm-9-C) and two 10-fold structures (Cm-10-D and Cm-10-E), and for Th(IV) one 8-fold (Th-8-A), two 9-fold (Th-9-B and Th-9-C) and three 10-fold ones (Th-10-D, Th-10-E and Th-10-F). These structures were extracted from in liquid water simulations being representative of the stoichiometries obtained in the previous SSM dynamics.

CASSCF/CASPT2 calculations confirm that the Cm(III) species are single-reference systems, as expected, since Cm(III) has the electronic configuration $[Rn]5f^{7}6d^{0}7s^{0}$. Th(IV) has the electronic configuration $[Rn]5f^{0}6d^{0}7s^{0}$ and thus we performed HF/MP2 calculations to have a comparison with a wave-function based method.

As we show in supporting information (Tables S1–S3, ESI†), relative energies between isomers with the same number of first shell water molecules and electronic energy differences between different stoichiometries strengthen the view that DFT is able to catch key features of Cm(III) and Th(IV) hydration. We should note that in the gas phase (for which we can compare

Table 1 Summary of NBO analysis for Cm(III)–water clusters. NC is for natural charge, NSD for natural spin density and SO for second order. In the last column we summarize the main contribution between occupied and empty orbitals as for SO perturbation theory from NBO. In the SO column LP stands for "lone pair" and * denotes an antibonding orbital (more details in Table S5 (ESI)). In parentheses we show the character of the Cm antibonding lone pair

	Valence on Cm	Cm NC	Cm NSD	SO interaction
CM-8-A	$7s^{0.16}5f^{7}6d^{0.52}$	2.27	6.99	LP_O → LP*Cm(7s) LP_O → LP*Cm(6d)
CM-8-B	$7s^{0.15}5f^{7}6d^{0.49}$	2.30	6.99	LP_O → LP*Cm(7s) LP_O → LP*Cm(6d)
CM-9-C	$7s^{0.16}5f^{7}6d^{0.57}$	2.20	6.99	LP_O → LP*Cm(7s) LP_O → LP*Cm(6d)
CM-10-D	$7s^{0.16}5f^{7}6d^{0.60}$	2.18	6.99	LP_O → LP*Cm(7s) LP_O → LP*Cm(6d)
CM-10-E	$7s^{0.17}5f^{7}6d^{0.59}$	2.20	6.99	LP_O → LP*Cm(7s) LP_O → LP*Cm(6d)

DFT with CASSCF/CASPT2 and MP2 calculations) the BLYP functional tends to underestimate the energy difference, in particular for the two 10-fold Cm(III)-water clusters, and M05-2X shows better agreement with CASPT2 and MP2 than the popular B3LYP functional.

We performed an NBO analysis on the DFT electronic structure. We will discuss only the M05-2X results, since the B3LYP and BLYP results are quite similar. We also inspected the molecular orbitals obtained from the wave-function based calculations. The results are qualitatively similar between Cm(III) and Th(IV) even if some interesting difference emerges. In Table 1 we report the most relevant NBO results for Cm(III) (more details are presented in Table S4 (ESI†)). The natural charge on Cm is slightly less than the formal one (3+), since some charge from the surrounding water molecules goes to the ion. The spin density is *ca.* 7 since the 7s and 6d valence orbitals are nearly empty. According to this analysis, no covalent interaction occurs between Cm and O. From second-order perturbation theory analysis of the Fock matrix in the NBO basis some interaction between the lone pairs of oxygen atoms and the empty orbitals of Cm (s and d mainly) is detected. This interaction is purely ionic and relatively small. Furthermore, no relevant differences are obtained by changing the number of water molecules in the first shell of the central ion. According to the CASSCF calculations, the seven singly occupied orbitals are atomic-like 5f (see Tables S5 and S6 (ESI†) for details on molecular orbitals). Notably, if we calculate the HOMO–LUMO energy gaps from different structures (the energy of the pseudo-canonical orbitals) we obtain values that are almost constant. The maximum difference is about three times smaller (5.7 kcal mol^{-1}) if compared with the spread of LUMO (18.76 kcal mol^{-1}) or HOMO (16.94 kcal mol^{-1}) orbitals between different Cm(III)–water clusters. This "alignment" of HOMO–LUMO difference regardless of the structure is similar to what recently found for hydrogen levels in semiconductors, insulators and solutions.[83]

For Th(IV) the situation is slightly different, as shown in Table 2 and Tables S7 and S8 of (ESI†). The ion charge obtained from natural population analysis is in the 2.24–2.72 range, which is significantly smaller than the formal value (4+).

Table 2 Summary of NBO analysis for Th(IV)–water clusters. NC is for natural charge, BD for bond and SO for second order. BD and SO columns are an overview of what is detailed in Tables S6 and S7 (ESI) In the BD column we specify the % of each atom. In the SO column LP stands for "lone pair", BD for bond and * denotes an antibonding orbital. In parentheses we show the character of the antibonding Th lone pairs

	Valence	NC	BD	SO
TH-8-A	$7s^{0.14}5f^{0.05}6d^{0.67}$	2.72	Th(5%)–O(95%)	LP_O → LP*Th(ds) LP_O → LP*Th(dsf)
TH-9-B	$7s^{0.15}5f^{0.05}6d^{0.70}$	2.63	—	LP_O → LP*Th(df) LP_O → LP*Th(sdf) LP_O → LP*Th(df)
TH-9-C	$7s^{0.17}5f^{0.05}6d^{0.80}$	2.40	Th(5%)–O(95%)	LP_O → LP*Th(sdf) LP_O → BD*Th–O
TH-10-D	$7s^{0.17}5f^{0.05}6d^{0.84}$	2.29	Th(5%)–O(95%)	LP_O → LP*Th(df) LP_O → BD*Th–O
TH-10-E	$7s^{0.18}5f^{0.05}6d^{0.85}$	2.24	Th(5%)–O(95%)	LP_O → BD*Th–O LP_O → LP*Th(df)
TH-10-F	$7s^{0.18}5f^{0.05}6d^{0.84}$	2.26	Th(5%)–O(95%)	LP_O → BD*Th–O LP_O → LP*Th(df)

A strong interaction between Th(IV) and the water molecules emerges from NBO analysis. Bonds are found between Th and the O atoms, even if with highly ionic nature, as reflected by the high O contributions (>90%). When analyzing HOMO–LUMO differences, we do not see the same alignment as obtained for Cm(III)–water clusters (details are given in Tables S9 and S10 of (ESI†)). In fact, even just considering LUMO orbitals (that are most suitable when focusing on the properties of 5f orbitals, since they are in LUMOs for Th(IV)), the spread is now 17.69 kcal mol^{-1}, which is larger than what was observed for Cm. Even if 5f orbitals have little involvement in Th–water interaction, the larger spread (and the fact that some water orbitals are partially involved in these LUMOs) reflects the fact that in Th the orbital interaction is stronger than for Cm, as reported also by NBO analysis.

We should note that two different formal oxidation states, Cm(III) and Th(IV), lead to almost the same charge (see Tables 1 and 2). A similarity to the charge self-regulation effect found in transition metal insulators[84] can be invoked: by increasing the charge of the metal the interaction between the metal and ligand orbitals increase.

4. Conclusions

We have shown that the single sweep method can be combined with DFT-based molecular dynamics to provide thermodynamic information on hydration of ions in liquid water. This paves the way for using this method also to clarify the problem of coordination number (that is sometimes very problematic from both experimental and theoretical points of view) when studying ion hydration.

By comparing the hydration properties of two prototypical actinoid ions, Cm(III) and Th(IV), with a different charge, we described the differences between these two systems. We showed that the interaction between these actinide ions and water molecules is mainly ionic and the Coulomb interaction grounds the difference in the hydration between these two ions. This is clearly reflected in the different behaviors of the ion

coordination free energy landscapes. In particular, for Cm(III) we found that the system can easily span the ion coordination surface, thus providing a not uniquely defined coordination. On the other hand, Th(IV) shows a much more stable coordination. Interestingly, Cm(III) seems to behave like an insulator,[83] since the HOMO–LUMO gap does not change as the water arrangement changes (in both coordination number and geometry). Furthermore, from a general perspective, actinoid ions behave similarly to transition metals in insulators through a charge self-regulation: by increasing the oxidation state the orbital energy goes down and empty orbitals can better accept back-bonding from donor groups (lone pairs of water in this case). This was found in the case of light actinoids making An–O bonds[85] and here we suggest a possible general mechanism valid also for non-covalent interactions.

Our results thus provide the following picture for the two ions: (i) in the case of Cm(III) there is a flat surface between 8-, 9- and 10-fold structures, and thus the hydration is characterized by a dynamical exchange where the ''most probable'' state corresponds to a 9-fold structure where the 9-th water molecule is leaving; (ii) in the case of Th(IV) the 9-fold structure is the most stable one, probably in equilibrium with a 10-fold structure, but with a clear separation between the two structures.

These results confirm the results obtained for Cm(III) from different simulations.[27–29,35] In the case of Th(IV) we have shown for the first time from free energy calculations that the 9-fold structure is the most stable one from both thermodynamics and kinetics points of view.

This study thus provides a theoretical justification of why 3+ actinoid ions behave similarly in water (and are difficult to be separated): their interaction is mainly electrostatic and small differences in ionic radii are not enough to result in specific non-covalent interactions. On the other hand 4+ ions seem to be more promising: for Th(IV) we obtained a partial orbitalic interaction with surrounding water molecules that can be more actinoid specific. More investigations on 4+ actinoid ions are surely needed to design separation strategies based on ion–ligand non-covalent binding differentiation.

Acknowledgements

R.S., Y.J. and R.V. thank ANR 2010 JCJC 080701 ACLASOLV (Actinoids and Lanthanoids Solvation) for support. L.G. thanks the Director, Office of Basic Energy Sciences, U.S. Department of Energy, under Contract No. USDOE/DE-SC002183. We acknowledge GENCI (grant x2012071870 and x20131870) for computing time. We also thank Dr M. Monteferrante and Dr S. Bonella for kindly providing code sources to obtain free energy curves.

References

1 H. Ohtaki and T. Radnai, *Chem. Rev.*, 1993, **93**, 1157–1204.
2 L. Helm and A. E. Merbach, *Chem. Rev.*, 2005, **105**, 1923–1960.
3 Y. Marcus, *Chem. Rev.*, 1988, **88**, 1475–1498.
4 P. D'Angelo and R. Spezia, *Chem.–Eur. J.*, 2012, **18**, 11162–11178.
5 T. S. Hofer, A. B. Pribil, B. R. Randolf and B. M. Rode, *Adv. Quantum Chem.*, 2010, **59**, 213.
6 B. J. Borah and S. Yashonath, *J. Chem. Phys.*, 2010, **133**, 114504.
7 P. K. Ghorai, S. Yashonath and R. M. Lynden-Bell, *J. Phys. Chem. B*, 2005, **109**, 8120–8124.
8 S. Koneshan, J. C. Rasaiah, R. M. Lynden-Bell and S. H. Lee, *J. Phys. Chem. B*, 1998, **102**, 4193–4204.
9 K. B. Møller, R. Rey, M. Masia and J. T. Hynes, *J. Chem. Phys.*, 2005, **122**, 114508.
10 R. Brooks, A. Davies, G. Ketwaroo and P. A. Madden, *J. Phys. Chem. B*, 2005, **109**, 6485–6490.
11 M. Salanne, C. Simon, P. Turq and P. A. Madden, *J. Phys. Chem. B*, 2007, **111**, 4678–4684.
12 F. Martelli, R. Vuilleumier, J.-P. Simonin and R. Spezia, *J. Chem. Phys.*, 2012, **137**, 164501.
13 P. D'Angelo, A. Zitolo, V. Migliorati, G. Chillemi, M. Duvail, P. Vitorge, S. Abadie and R. Spezia, *Inorg. Chem.*, 2011, **50**, 4572–4579.
14 T. Kowall, F. Foglia, L. Helm and A. E. Merbach, *J. Am. Chem. Soc.*, 1995, **117**, 3790–3799.
15 C. Terrier, P. Vitorge, M.-P. Gaigeot, R. Spezia and R. Vuilleumier, *J. Chem. Phys.*, 2010, **133**, 044509.
16 M. Duvail, P. D'Angelo, M.-P. Gaigeot, P. Vitorge and R. Spezia, *Radiochim. Acta*, 2009, **97**, 339–346.
17 L. Maragliano and E. Vanden-Eijden, *J. Chem. Phys.*, 2008, **128**, 184110.
18 M. Monteferrante, S. Bonella, S. Meloni, E. Vanden-Eijnden and G. Ciccotti, *Sci. Model. Simul.*, 2008, **15**, 187–206.
19 M. Monteferrante, S. Bonella, S. Meloni and G. Ciccotti, *Mol. Simul.*, 2009, **35**, 1116.
20 L. Maragliano, G. Cottone, G. Ciccotti and E. Vanden-Eijnden, *J. Am. Chem. Soc.*, 2010, **132**, 1010–1017.
21 G. Ciccotti and S. Meloni, *Phys. Chem. Chem. Phys.*, 2011, **13**, 5952–5959.
22 M. Monteferrante, S. Bonella and G. Ciccotti, *Phys. Chem. Chem. Phys.*, 2011, **13**, 10546–10555.
23 A. Laio and M. Parrinello, *Proc. Natl. Acad. Sci. U. S. A.*, 2002, **99**, 12562–12566.
24 G. Brancato and V. Barone, *J. Phys. Chem. B*, 2011, **115**, 12875–12878.
25 T. Ikeda, M. Hirata and T. Kimura, *J. Chem. Phys.*, 2005, **122**, 244507.
26 M. Duvail, F. Martelli, P. Vitorge and R. Spezia, *J. Chem. Phys.*, 2011, **135**, 044503.
27 P. D'Angelo, F. Martelli, R. Spezia, A. Filipponi and M. A. Denecke, *Inorg. Chem.*, 2013, **52**, 10318–10324.
28 D. Hagberg, E. Bednarz, N. M. Edelstein and L. Gagliardi, *J. Am. Chem. Soc.*, 2007, **129**, 14136–14137.
29 F. Réal, M. Trumm, V. Vallet, B. Schimmelpfennig, M. Masella and J.-P. Flament, *J. Phys. Chem. B*, 2010, **114**, 15913–15924.
30 S. Skanthakumar, M. R. Antonio, R. E. Wilson and L. Soderholm, *Inorg. Chem.*, 2007, **46**, 3485–3491.
31 P. Lindqvist-Reis, R. Klenze, G. Schubert and T. Fanghanel, *J. Phys. Chem. B*, 2005, **109**, 3077–3083.

32 P. Lindqvist-Reis, C. Apostolidis, J. Rebizant, A. Morgenstern, R. Klenze, O. Walter, T. Fanghanel and R. Haire, *Angew. Chem., Int. Ed.*, 2007, **46**, 919–922.
33 T. Yang and B. E. Bursten, *Inorg. Chem.*, 2006, **45**, 5291–5301.
34 R. Atta-Fynn, E. J. Bylaska, G. K. Schenter and W. A. de Jong, *J. Phys. Chem. A*, 2011, **115**, 4665–4677.
35 R. Atta-Fynn, E. J. Bylaska and W. A. de Jong, *J. Phys. Chem. Lett.*, 2013, **4**, 2166–2170.
36 H. Moll, M. A. Denecke, F. Jalilehvand, M. Sandstrom and I. Grenthe, *Inorg. Chem.*, 1999, **38**, 1795–1799.
37 N. Torapava, I. Persson, L. Eriksson and D. Lundberg, *Inorg. Chem.*, 2009, **48**, 11712–11723.
38 R. E. Wilson, S. Skanthakumar, P. C. Burns and L. Soderholm, *Angew. Chem., Int. Ed.*, 2007, **46**, 8043–8045.
39 R. Spezia, C. Beuchat, R. Vuilleumier, P. D'Angelo and L. Gagliardi, *J. Phys. Chem. B*, 2012, **116**, 6465–6475.
40 T. Yang, S. Tsushima and A. Suzuki, *J. Phys. Chem. A*, 2001, **105**, 10439–10445.
41 F. Réal, M. Trumm, B. Schimmelpfennig, M. Masella and V. Vallet, *J. Comput. Chem.*, 2013, **34**, 707–719.
42 M. Monteferrante, S. Bonella, S. Meloni, E. Vanden-Eijnden and G. Ciccotti, *Sci. Model. Simul.*, 2008, **15**, 187–206.
43 R. Car and M. Parrinello, *Phys. Rev. Lett.*, 1985, **55**, 2471–2474.
44 A. D. Becke, *Phys. Rev. A: At., Mol., Opt. Phys.*, 1988, **38**, 3098.
45 C. Lee, W. Yang and R. G. Parr, *Phys. Rev. B: Condens. Matter Mater. Phys.*, 1988, **37**, 785.
46 N. Troullier and J. L. Martins, *Phys. Rev. B: Condens. Matter Mater. Phys.*, 1991, **43**, 1993–2006.
47 L. Kleinman and D. M. Bylander, *Phys. Rev. Lett.*, 1982, **48**, 1425–1428.
48 D. Marx and J. Hutter, *Ab Initio Molecular Dynamics: Basic Theory and Advanced Methods*, Cambridge University Press, Cambridge, U.K., 2009; CPMD libraries freely available at www.cpmd.org/download.
49 O. A. von Lilienfeld, I. Tavernelli, U. Rothlisberger and D. Sebastiani, *Phys. Rev. Lett.*, 2004, **93**, 153004.
50 P. D'Angelo, V. Migliorati and L. Guidoni, *Inorg. Chem.*, 2010, **49**, 4224–4231.
51 S. Raugei and M. LKlein, *Chem. Phys.*, 2002, **116**, 196–202.
52 L. Maragliano and E. Vanden-Eijnden, *Chem. Phys. Lett.*, 2006, **426**, 168–175.
53 S. Nosé, *Mol. Phys.*, 1984, **52**, 255.
54 R. Spezia and R. Vuilleumier, *Mol. Phys.*, 2013, **111**, 3478–3485.
55 J. Hutter, A. Alavi, T. Deutsch, M. Bernasconi, S. Goedecker, D. Marx, M. A. Tuckerman and M. Parrinello, *CPMD, version 3.12*, IBM Research Division, IBM Corp and Max Planck Institute, Stuttgart, Germany, 2004.
56 W. Kuechle, M. Dolg, H. Stoll and H. Preuss, *J. Chem. Phys.*, 1994, **100**, 7535.
57 (*a*) X. Cao, M. Dolg and H. Stoll, *J. Chem. Phys.*, 2003, **118**, 487; (*b*) X. Cao and M. Dolg, *THEOCHEM*, 2004, **673**, 203.
58 (*a*) A. D. Becke, *J. Chem. Phys.*, 1993, **98**, 5648; (*b*) C. Lee, W. Yang and R. G. Parr, *Phys. Rev. B: Condens. Matter Mater. Phys.*, 1998, **37**, 785–789; (*c*) S. H. Vosko, L. Wilk and M. Nusair, *Can. J. Phys.*, 1980, **58**, 1200–1211; (*d*) P. J. Stephens, F. J. Devlin, C. F. Chabalowski and M. J. Frisch, *J. Phys. Chem.*, 1994, **98**, 11623–11627.
59 Y. Zhao, N. E. Schultz and D. G. Truhlar, *J. Chem. Theory Comput.*, 2006, **2**, 364–382.
60 Y. Jeanvoine and R. Spezia, *J. Phys. Chem. A*, 2009, **113**, 7878–7887.
61 Y. Jeanvoine and R. Spezia, *THEOCHEM*, 2010, **954**, 7–15.
62 J. P. Foster and F. Weinhold, *J. Am. Chem. Soc.*, 1980, **102**, 7211–7218.
63 A. E. Reed and F. Weinhold, *J. Chem. Phys.*, 1983, **78**, 4066–4073.
64 A. E. Reed, R. B. Weinstock and F. Weinhold, *J. Chem. Phys.*, 1985, **83**, 735–746.
65 E. D. Glendening, J. K. Badenhoop, A. E. Reed, J. E. Carpenter, J. A. Bohmann, C. M. Morales and F. Weinhold, *NBO 5.9*, Theoretical Chemistry Institute, University of Wisconsin, Madison, WI, 2009; http://www.chem.wisc.edu/~nbo5.
66 G. Karlström, R. Lindh, P.-A. Malmqvist, B. O. Roos, U. Ryde, V. Veryazov, P.-O. Widmark, M. Cossi, B. Schimmelpfennig, P. Neogrady and L. Seijo, *Comput. Mater. Sci.*, 2003, **287**, 222–239.
67 B. O. Roos, P. R. Taylor and P. E. M. Siegbahn, *Chem. Phys.*, 1980, **48**, 157–173.
68 K. Andersson, P.-A. Malmqvist and B. O. Roos, *J. Chem. Phys.*, 1992, **96**, 1218–1226.
69 L. Gagliardi, M. C. Heaven, J. W. Krogh and B. O. Roos, *J. Am. Chem. Soc.*, 2005, **127**, 86–91.
70 L. Gagliardi, *J. Am. Chem. Soc.*, 2003, **125**, 7504–7505.
71 L. Gagliardi, *Theor. Chem. Acc.*, 2006, **116**, 307–315.
72 L. Gagliardi and C. J. Cramer, *Inorg. Chem.*, 2006, **45**, 9442–9447.
73 L. Gagliardi, G. La Manna and B. O. Roos, *Faraday Discuss.*, 2003, **124**, 63–68.
74 L. Gagliardi, P. Pyykko and B. O. Roos, *Phys. Chem. Chem. Phys.*, 2005, **7**, 2415–2417.
75 L. Gagliardi and B. O. Roos, *Chem. Soc. Rev.*, 2007, **36**, 893–903.
76 I. Infante, L. Gagliardi and G. E. Scuseria, *J. Am. Chem. Soc.*, 2008, **130**, 7459–7465.
77 I. Infante, L. Gagliardi, X. F. Wang and L. Andrews, *J. Phys. Chem. A*, 2009, **113**, 2446–2455.
78 I. Infante, J. Raab, J. T. Lyon, B. Liang, L. Andrews and L. Gagliardi, *J. Phys. Chem. A*, 2007, **111**, 11996–12000.
79 I. Persson, P. D'Angelo, S. De Panfilis, M. Sandström and L. Eriksson, *Chem.–Eur. J.*, 2008, **14**, 3056–3066.
80 S. Tsuchima, *J. Phys. Chem. B*, 2008, **112**, 7080–7085.
81 Y. Okamoto, Y. Mochizuki and S. Tsushima, *Chem. Phys. Lett.*, 2003, **373**, 213–217.
82 R. Ayala, R. Spezia, R. Vuilleumier, J. M. Martinez, R. R. Pappalardo and E. Sanchez Marcos, *J. Phys. Chem. B*, 2010, **114**, 12866–12874.
83 C. G. Van de Walle and J. Neugebauer, *Nature*, 2003, **423**, 626–628.
84 H. Raebiger, S. Lany and A. Zunger, *Nature*, 2008, **453**, 763–766.
85 I. D. Prodan, G. E. Scuseria and R. L. Martin, *Phys. Rev. B: Condens. Matter Mater. Phys.*, 2007, **76**, 033101.

